УДК 532.517.4; 533; 533.6.011.5

Ye. Moisseyeva

Al-Farabi Kazakh National University, Almaty, Kazakhstan
E-mail: K.Moisseyeva@gmail.com

Analysis of ENO scheme slope limiters

The interaction of the three-dimensional supersonic turbulent air flow with the transversely injected hydrogen jet is numerically simulated by solving the Reynolds-averaged Navier-Stokes equations using the ENO (essentially non-oscillatory) scheme of the third order of accuracy. Since the choice of the limiter functions significantly affects the accuracy of the problem, preliminary test problems are solved to validate numerical method and choose optimal slope limiter. Analysis of the different variations of the limiter functions for developed algorithm was done to define optimal function produced the smallest solution spreading. Then, the effect of the different variations of the limiter functions for developed algorithm on the mixing layer is studied since the exact calculation of the mass concentration spreading is important issue in combustion problem modeling. Also, by numerical experiments the effect of the slope limiters on the shock-wave structure formation is studied. It was shown that choice of some limiters can result in excessive expansion of the mixing layer, that is important issue in numerical modeling of scramjet engine. As result, the optimal limiter function which produces the smallest spread of solution for the spatial problem was defined. Also the mechanism of the formation of vortices in front of the injected jet and behind that is studied.

Key words: supersonic flow, multicomponent gas, ENO scheme, limiters, Navier- Stokes equations.

Е.С. Моисеева

Анализ ограничителей наклона ENO-схемы

Численно моделируется взаимодействие сверхзвукового турбулентного течения воздуха с поперечно вдуваемой струей водорода путем решения осредненных по Рейнольдсу уравнений Навье-Стокса с использованием существенно неосциллирующей ENO-схемы третьего порядка точности. Поскольку выбор функций ограничителей оказывает значительное влияние на точность решения задачи, для валидации численного метода и выбора оптимального ограничителя наклона предварительно решаются тестовые задачи. Был проведен анализ различных комбинаций функций ограничителей в разработанном алгоритме с целью определить оптимальную функцию, приводящую к наименьшему размыванию решения. После этого изучается влияние выбранных комбинаций функций ограничителей в разработанном алгоритме на слой смешения, поскольку точный расчет распространения массовых концентраций является важным аспектом при моделировании проблем горения. Также с помощью численных экспериментов изучается влияние ограничителей наклона на образование ударно-волновой структуры. Показано, что выбор некоторых ограничителей может привести к чрезмерному расширению слоя смешения, что является важным при численном моделировании сверхзвуковых ПВРД. В результате был определен оптимальный ограничитель, приводящий к наименьшему размазыванию решения для рассматриваемой пространственной задачи. Также в работе изучается механизм формирования вихрей перед вдуваемой струей и за ней.

Ключевые слова: сверхзвуковое течение, многокомпонентный газ, ENO-схема, ограничители, уравнения Навье-Стокса.

Е.С. Моисеева

ENO-сұлбасының көлбеуінің тежегішінің талдануы

Рейнольдс бойынша орташаланған Навье-Стокс теңдеуін шешуге үшінші ретті ENO-сұлбасын қолдану арқылы жылдамдығы дыбыс жылдамдығынан жоғары турбуленттік ағын мен көлденең үрленетін сутегі ағыншасының өзара әсерлесуінің сандық моделі жасалды. Шектеуші функциясын таңдау есепті шешу дәлдігіне едәуір әсер ететіндіктен, сандық әдістің сенімділігін тексеру үшін және шектеушінің көлбеулігінің оңтайлылығын таңдау үшін алдын ала тесттік есептер шығарылады. Тиімді функцияны анықтау мақсатында құрастырылған алгоритмде шектеуші функцияға әр түрлі әдістердің анализі жасалды. Содан соң таңдалған шектеуші функцияның әдістерінің құрастырылған алгоритмдегі араласу қабатына әсері зерттеледі. Сонымен бірге сандық тәжірибелер көмегімен шектеуші көлбеуінің екпінді толқындылықтың пайда болу құрылымына әсерін зерттеледі. Кейбір таңдалған шектеушілер араласу қабатының шектен тыс ұлғаюына әкеп соғатыны көрсетілді. Нәтижесінде қарастырылып отырылған кеңістіктік есеп үшін ең аз жағылып кетудің оңтайлы шектеуіші анықталды. Сонымен бірге жұмыста үрлеу ағынына дейін және үрлеу ағынынан кейінгі ұйытқыманың пайда болу механизмі зерттеледі.

Түйін сөздер: жылдамдығы дыбыс жылдамдығынан жоғары ағындар, көпкомпонентті газ, ENO-сұлба, шектеуші, Навье-Стокс теңдеуі.

Introduction

Currently, in numerical simulations of supersonic flows the main tool is the essentially non-oscillating schemes: ENO and WENO (weighted ENO) schemes. These schemes are well adapted for solving the Navier-Stokes equations for a perfect gas [3, 2, 1]. Multicomponent gas flow modeling is important for practical application, but these schemes are less adapted for such problems. The ENO scheme based on the Godunov method was developed and its applicability to the problem of transverse jet injection into a supersonic turbulent multicomponent gas flow in a flat channel was shown by the authors in [4].

As well known, piece-wise function distribution inside a cell is used during construction of high-order methods in space. To define the function on the cell boundary by its value in the cell center it is necessary to introduce of a reconstruction procedure. Conditions imposed on the function slope is modified by limiters [5]. The main difficulty is related with ambiguity of the choice of these functions. Most of the research on effect of limiter choice on the solution has been in one dimension [6, 7, 8]. Different ways of reconstruction in 2D and 3D are set out in [5, 10, 9]. It should be noticed that multidimensional reconstructions do not have strict justification. Applicability of these methods should be investigated in every particular case.

The aim of this paper is numerical modeling of a spatial turbulent steady flowfield generated by transverse hydrogen injection into a supersonic cross-flow (Fig.1). To solve this problem, numerical method developed by authors in [4], based on the third order ENO scheme, is adapted for three-dimensional case. Additionally, the effective adiabatic parameter of the gas mixture is introduced. It allows one to calculate the derivatives of the pressure with respect to independent variables for determining the Jacobian matrices, and

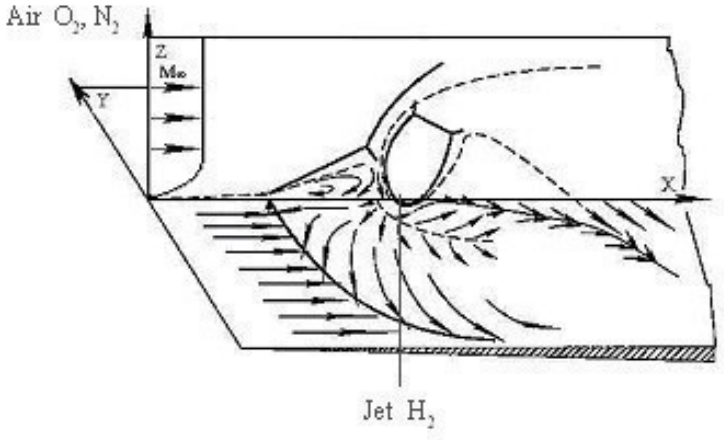

Figure 1. Schematics of flowfield

thus to construct an efficient implicit algorithm of the solution. Effect of the limiter choice in numerical algorithms on the mixing layer is studied since the exact calculation of the mass concentrations spread is an important issue in combustion problems modeling.

Problem formulation

Basic equations for the problem are the system of the three-dimensional Reynolds averaged Navier-Stokes equations for the compressible turbulent multicomponent gas in the Cartesian coordinate system written in conservative form as

$$\frac{\partial \vec{U}}{\partial t} + \frac{\partial \left(\vec{E} - \vec{E}_v\right)}{\partial x} + \frac{\partial \left(\vec{F} - \vec{F}_v\right)}{\partial y} + \frac{\partial \left(\vec{G} - \vec{G}_v\right)}{\partial z} = 0, \tag{1}$$

$$\vec{U} = (\rho, \rho u, \rho v, \rho w, E_t, \rho Y_k)^T, \vec{E} = \left(\rho u, \rho u^2 + p, \rho uv, \rho uw, (E_t + p)\, u\right)^T,$$

$$\vec{F} = \left(\rho v, \rho uv, \rho v^2 + p, \rho vw, (E_t + p)\, v\right)^T, \vec{G} = \left(\rho w, \rho uw, \rho vw, \rho w^2 + p, (E_t + p)\, w\right)^T.$$

$$\vec{E}_v = (0, \tau_{xx}, \tau_{xy}, \tau_{xz}, u\tau_{xx} + v\tau_{xy} + w\tau_{xz} - q_x, J_{kx})^T,$$

$$\vec{F}_v = (0, \tau_{xy}, \tau_{yy}, \tau_{yz}, u\tau_{xy} + v\tau_{yy} + w\tau_{yz} - q_y, J_{ky})^T,$$

$$\vec{G}_v = (0, \tau_{xz}, \tau_{yz}, \tau_{zz}, u\tau_{xz} + v\tau_{yz} + w\tau_{zz} - q_z, J_{kz})^T,$$

where $\tau, \vec{q}$ and $\vec{J}_k$ are viscous stress tensor, heat flux and diffusion flux, respectively.

Viscosity coefficient is defined as a sum of laminar and turbulent viscosity coefficients: $\mu = \mu_l + \mu_t$. μ_l is determined by Wilke formula. μ_t is determined by the Baldwin-Lomax turbulence model. Near the wall $\mu_t = \rho l^2 |\Omega|$, $l = \kappa z \left(1 - e^{-z^+/A}\right)$, $\kappa = 0.41$, $A = 26$. $|\Omega|$ is the vorticity. In the outer region $\mu_t = 0.0168 \rho V_0 L_0$, $V_0 = min\left(F_{max}; 0.25 q_{dif}^2 / F_{max}\right)$, $L_0 = 1.6$, $z_{max} I^k$, $q_{dif} = max\left(\vec{V}\right) - min\left(\vec{V}\right)$, $F_{max} = max\left(\|\Omega\| l/\kappa\right)$. $I^k = \left[1 + 5.5\left(0.3 z/z_{max}\right)^6\right]^{-1}$ is the Klebanov factor. z_{max} corresponds to F_{max}. $\vec{V}$ is the velocity.

Pressure and total energy are defined by

$$p = \frac{\rho T}{\gamma_\infty M_\infty^2} \sum_{k=1}^{N} \frac{Y_k}{W_k},\ E_t = \frac{\rho}{\gamma_\infty M_\infty^2} \sum_{k=1}^{N} Y_k h_k - p + \frac{1}{2}\rho(u^2 + v^2 + w^2)$$

In the system (1) $u,\ v,\ w,\ \rho,\ T$ represent components of velocity vector, density and temperature, respectively. $Y_k,\ W_k$ and h_k are mass fraction, molecular weight and specific enthalpy of the kth species, where Y_1, Y_2, Y_3 stand for mass fraction of H_2, O_2, N_2, respectively. γ is adiabatic parameter, M is Mach number. Index 0 indicates jet parameters and index ∞ indicates parameters of the main flow. The system (1) is written in a nondimensional form. Constitutive parameters are parameters of the main flow at the inlet ($u_\infty,\ \rho_\infty,\ T_\infty$). The injector diameter d is chosen as the characteristic length.

Boundary conditions. On the flow field entrance, the parameters of the free stream are given

$p = p_\infty,\ T = T_\infty,\ u = M_\infty\sqrt{\frac{\gamma_\infty R_0 T_\infty}{W_\infty}},\ v = w = 0,\ Y_k = Y_{k\infty},\ W_k = W_{k\infty},\ x = 0,\ 0 \le y \le H_y,\ 0 \le z \le H_z$. Also boundary layer is given near the wall, longitudinal velocity component is approximated by 1/7th power law.

On the injector, the parameters of the jet are given

$p = np_\infty,\ T = T_0,\ u = v = 0,\ w = M_0\sqrt{\frac{\gamma_0 R_0 T_0}{W_0}},\ Y_k = Y_{k0},\ W_k = W_{k0},\ z = 0,\ |x^2 + y^2| \le R$, where n is the pressure ratio.

The adiabatic no-slip boundary condition on the wall is specified

$u = v = w = 0,\ \frac{\partial T}{\partial z} = \frac{\partial p}{\partial z} = \frac{\partial Y_k}{\partial z} = 0,\ z = 0,\ 0 \le y \le H_y,\ 0 \le x \le H_x$

The symmetry boundary conditions on the symmetry faces are specified

$\frac{\partial u}{\partial z} = \frac{\partial v}{\partial z} = w = 0,\ \frac{\partial T}{\partial z} = \frac{\partial p}{\partial z} = \frac{\partial Y_k}{\partial z} = 0,\ z = H_z,\ 0 \le x \le H_x,\ 0 \le y \le H_y,$

$\frac{\partial u}{\partial y} = \frac{\partial v}{\partial y} = \frac{\partial w}{\partial y} = 0,\ \frac{\partial T}{\partial y} = \frac{\partial p}{\partial y} = \frac{\partial Y_k}{\partial y} = 0,\ y = 0,\ y = H_y,\ 0 \le x \le H_x,\ 0 \le z \le H_z.$

The non-reflecting boundary conditions are adopted on the flow field exit [11]. Here $H_x,\ H_y$ and H_z are the length, width and height of computational domain, respectively. R is the injector radius.

Method of solution

In the regions of large gradients (in the boundary layer, near the wall and on the jet exit) condensation of the grid is introduced. Then the system (1) in the transformed coordinate system may be written as

$$\frac{\partial \tilde{U}}{\partial t} + \frac{\partial \tilde{E}}{\partial \xi} + \frac{\partial \tilde{F}}{\partial \eta} + \frac{\partial \tilde{G}}{\partial \zeta} = \frac{\partial \tilde{E}_{v2}}{\partial \xi} + \frac{\partial \tilde{E}_{vm}}{\partial \xi} + \frac{\partial \tilde{F}_{v2}}{\partial \eta} + \frac{\partial \tilde{F}_{vm}}{\partial \eta} + \frac{\partial \tilde{G}_{v2}}{\partial \zeta} + \frac{\partial \tilde{G}_{vm}}{\partial \zeta} \tag{2}$$

where $\tilde{U} = \left(\frac{1}{J}\right)\vec{U},\ \tilde{E} = \left(\frac{\xi_x}{J}\right)\vec{E},\ \tilde{F} = \left(\frac{\eta_y}{J}\right)\vec{F},\ \tilde{G} = \left(\frac{\zeta_z}{J}\right)\vec{G},\ \tilde{E}_{v2} = \left(\frac{\xi_x}{J}\right)\vec{E}_{v2},$

$\tilde{F}_{v2} = \left(\frac{\eta_y}{J}\right)\vec{F}_{v2},\ \tilde{G}_{v2} = \left(\frac{\zeta_z}{J}\right)\vec{G}_{v2},\ \tilde{E}_{vm} = \left(\frac{\xi_x}{J}\right)\vec{E}_{vm},\ \tilde{F}_{vm} = \left(\frac{\eta_y}{J}\right)\vec{F}_{vm},\ \tilde{G}_{vm} = \left(\frac{\zeta_z}{J}\right)\vec{G}_{vm}.$

$J = \frac{\partial(\xi, \eta, \zeta)}{\partial(x, y, z)}$ is the Jacobian of the transformation. The diffusion terms are represented by the sum of second derivative terms (which indicated by index $v2$) and mixed derivative terms (which indicated by index vm).

For numerical solution of the system (2) ENO scheme of the third order is used for spatial discretization. Method of numerical algorithm construction was shown in [4]. In accordance with the principle of the ENO scheme, the one-step finite difference scheme for the time integration of the system (2) is presented formally as

$$\Delta\tilde{U}^{n+1} + \Delta t \left\{ \left(\hat{A}^+ + \hat{A}^-\right) \frac{\partial \vec{E}^m}{\partial \xi} + \left(\hat{B}^+ + \hat{B}^-\right) \frac{\partial \vec{F}^m}{\partial \eta} + \left(\hat{C}^+ + \hat{C}^-\right) \frac{\partial \vec{G}^m}{\partial \zeta} - \right.$$
$$\left. - \left[\frac{\partial \left(\tilde{E}_{v2}^{n+1} + \tilde{E}_{vm}^{n}\right)}{\partial \xi} + \frac{\partial \left(\tilde{F}_{v2}^{n+1} + \tilde{F}_{vm}^{n}\right)}{\partial \eta} + \frac{\partial \left(\tilde{G}_{v2}^{n+1} + \tilde{G}_{vm}^{n}\right)}{\partial \zeta} \right] \right\} = O\left(\frac{1}{2}\Delta t^2\right) \quad (3)$$

Here $\vec{E}^m,\ \vec{F}^m,\ \vec{G}^m$ are the modified fluxes at the node point (i,j,k), which consist of the original convective vectors $(\tilde{E},\ \tilde{F},\ \tilde{G})$ and additional terms of the high order of accuracy $(\vec{E}_\xi, \vec{D}_\xi,\ \vec{E}_\eta, \vec{D}_\eta,\ \vec{E}_\zeta, \vec{D}_\zeta)$: $\vec{E}^m = \tilde{E}^{n+1} + \left(\vec{E}_\xi + \vec{D}_\xi\right)^n$,

where $\vec{E}_{\xi ijk} = limiter1(\bar{E}_{\xi i-1/2jk},\ \bar{E}_{\xi i+1/2jk})$

$$\vec{D}_{\xi ijk} = \begin{cases} limiter2(\Delta_- \hat{D}_{\xi i-1/2jk},\ \Delta_+ \hat{D}_{\xi i-1/2jk}) & \text{if} \left|\Delta_- \tilde{U}_{ijk}\right| \le \left|\Delta_+ \tilde{U}_{ijk}\right| \\ limiter2(\Delta_- \bar{D}_{\xi i+1/2jk},\ \Delta_+ \bar{D}_{\xi i+1/2jk}) & \text{if} \left|\Delta_- \tilde{U}_{ijk}\right| > \left|\Delta_+ \tilde{U}_{ijk}\right| \end{cases} \text{for } \lambda > 0$$

$$\vec{D}_{\xi ijk} = \begin{cases} limiter2(\Delta_- \bar{D}_{\xi i-1/2jk},\ \Delta_+ \bar{D}_{\xi i-1/2jk}) & \text{if} \left|\Delta_- \tilde{U}_{ijk}\right| \le \left|\Delta_+ \tilde{U}_{ijk}\right| \\ limiter2(\Delta_- \hat{D}_{\xi i+1/2jk},\ \Delta_+ \hat{D}_{\xi i+1/2jk}) & \text{if} \left|\Delta_- \tilde{U}_{ijk}\right| > \left|\Delta_+ \tilde{U}_{ijk}\right| \end{cases} \text{for } \lambda \le 0$$

$$\bar{E}_{\xi i+1/2jk} = \frac{1}{2} sign(A_{i+1/2jk}) \left(I - \frac{\Delta t}{\Delta \xi} \left|A_{i+1/2jk}\right|\right),$$

$$\bar{D}_{\xi i+1/2jk} = \frac{1}{6} sign(A_{i+1/2jk}) \left[\left(\frac{\Delta t}{\Delta \xi} \left|A_{i+1/2jk}\right|\right)^2 - I\right],$$

$$\hat{D}_{\xi i+1/2jk} = \frac{1}{6} sign(A_{i+1/2jk}) \left[2I - 3\frac{\Delta t}{\Delta \xi} \left|A_{i+1/2jk}\right| + \left(\frac{\Delta t}{\Delta \xi} \left|A_{i+1/2jk}\right|\right)^2\right].$$

$\hat{A}^\pm = A^\pm / A$ and $\hat{A}^+ + \hat{A}^- = I$, $A^\pm = R\Lambda^\pm R^{-1} = R\left(\frac{\Lambda \pm |\Lambda|}{2}\right) R^{-1}$, I is the identity matrix, $A = \partial \vec{E} / \partial \vec{U}$ is Jacobi matrix.

Here the limiter functions $limiter1(a,b)$ and $limiter2(a,b)$ are associated with terms of the second and third order of accuracy, respectively. Functions $m(a,b)$, $minmod(a,b)$ or $superbee(a,b)$ are chosen as limiters, where

$$limiter1(a,b) = \dot{m}(a,b) = \begin{cases} \frac{1}{2}a & \text{if } |a| \le |b| \\ \frac{1}{2}b & \text{if } |a| > |b| \end{cases}$$

$$limiter1(a,b) = minmod(a,b) = \begin{cases} s \cdot min(|a|, |b|) & \text{if } sign(a) = sign(b) = s \\ 0 & \text{else} \end{cases} \quad (4)$$

$$limiter1(a,b) = superbee(a,b) = \begin{cases} \begin{cases} min(2a,b) & \text{if } |a| \le |b| \\ min(a,2b) & \text{if } |a| > |b| \end{cases} & \text{if } sign(a) = sign(b) \\ 0 & \text{else} \end{cases}$$

$limiter2(a,b)$ is determined in the same way, and the expressions for the fluxes $\vec{F}^m$ and $\vec{G}^m$ are written similarly to $\vec{E}^m$.

Numerical solution of the system (3) is performed in two steps. At the first step thermodynamic parameters $\rho,\ u,\ v,\ w,\ E_t$ and at the second step mass fractions Y_k are resolved. The upwind differences of the first order of accuracy have been used for the approximation of the first derivatives in system (3), and the central differences of the second order of accuracy have been used for the second derivatives. The obtained system of equations is solved with respect to the vector of thermodynamic parameters by the matrix sweep method, and the vector of mass fractions of the mixture is computed by tridiagonal inversion.

Test calculations

Despite the fact that the limiters are in Sweby diagram [12], the limiters have different effect on solution. So, preliminarily test problems were solved to validate numerical method and choose optimal limiter. First test problem is the Riemann problem for the Euler equations with the initial conditions: left from discontinuity $\rho_L = 8,\ p_L = 7.1,\ u_L = 0$, right from discontinuity $\rho_R = 1,\ p_R = 0.71,\ u_R = 0$, domain $1 \times 1 \times 1$, regular grid $101 \times 101 \times 101$, discontinuity is at $x_0 = 0.5$ [13].

Fig. 2 shows the results of the comparison of the exact solution and the numerical solution. Here solid line is for the exact solution, dotted line is for the numerical solution at $t = 0.2$, $N = 154$, $\frac{\Delta t}{\Delta x} = 0.1$. Figs. $2a$ and $2b$ show the results for the limiters

$$limiter1(a,b) = minmod(a,b),\ limiter2(a,b,) = 0; \tag{5a}$$

$$limiter1(a,b) = 1.5minmod(a,b),\ limiter2(a,b) = 1.5superbee(a,b) \tag{5b}$$

respectively, i.e. in the first case the problem was solved with the second order of accuracy, and in the second case it was solved with the third order. It is seen from the comparison that the calculated with the second order of accuracy curves is more smooth and have peaks, i.e. the results agree with test calculations of other authors [13, 14]. While the curves from Fig. $2b$, which is done with ENO, better agree with the exact solution.

As well known, when considering multidimensional problems the limiters are chosen similarly to one-dimensional problems in every direction. Although it is known [10], that negligent limiter choice in one direction can result in accuracy reduction and excessive dissipation for multidimensional case. Thereunder, problem of hydrogen mass fraction transfer is considered

$$\frac{\partial Y_k}{\partial t} + u\frac{\partial Y_k}{\partial x} + v\frac{\partial Y_k}{\partial y} + w\frac{\partial Y_k}{\partial z} = 0 \tag{6}$$

The velocities are regarded as constant and equal to 1. Initial condition for hydrogen mass fraction is given as cube cloud of lenth 2 (Fig.3a).

The results for the best limiters for the previous one-dimensional problem, i.e. (5b), show that in three-dimensional case such numerical coefficient are too high, so the limiters (5b) can

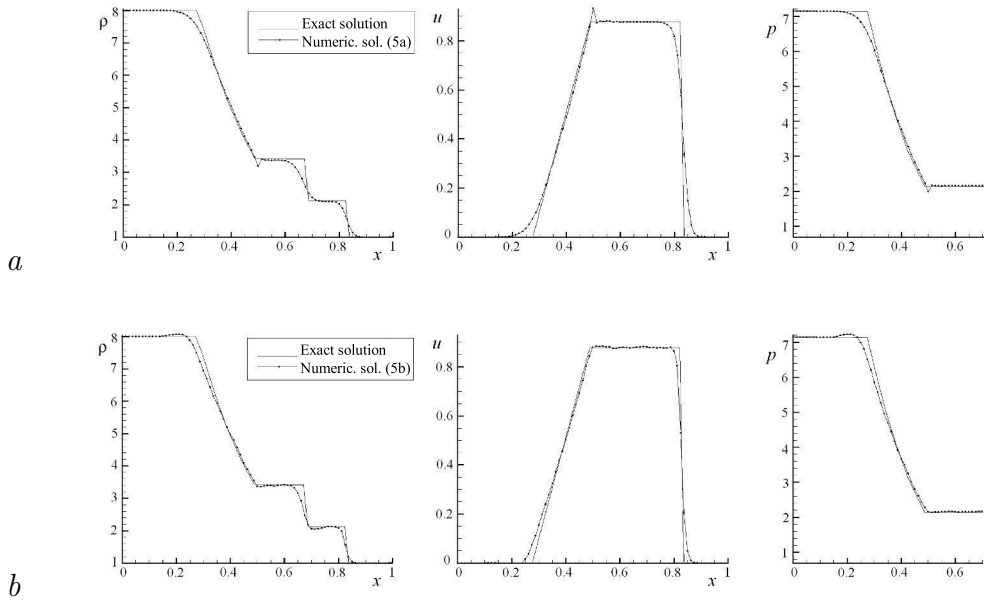

Figure 2. Numerical solution of Euler equations for Riemann problem: a – for the limiters $(5a)$; b – for the limiters $(5b)$

not be applied. Thus, suitable limiter choice for one-dimensional problem is not satisfactory for the three-dimensional problem.

In accordance with this, additional numerical experiments were done to choose satisfactory limiter choice. The limiters function were chosen from (4) as

$$limiter1(a,b) = minmod(a,b),\ limiter2(a,b,) = \dot{m}(a,b); \tag{7a}$$

$$limiter1(a,b) = 1.1superbee(a,b),\ limiter2(a,b) = \dot{m}(a,b) \tag{7b}$$

It follows from Fig.3b that the solution obtained with $(7a)$ significantly spreads the original solution, i.e. the limiters $(7a)$ reduce dissipative effects insufficiently. The original shape of cube is not preserved. The cloud becomes a symmetrical sphere at the time moment $t = 19$. On the contrary, slight change of the second order limiter $(7b)$ brings about significantly reduce of dissipative effects. The cube cloud is preserved its shape. Slight spread of the solution at the time moment $t = 19$ occurs (Fig.3c).

Results

The numerical computations of the original problem (1) were done with the parameters: time step $\Delta t = 0.01$, $Pr = 0.9$, $M_0 = 1$, $M_\infty = 4$, $4 \le n \le 15$, $Re = 10^4$; $H_x = 20$, $H_y = 15$, $H_z = 10$ calibres, $x_0 = 10$ calibres is the distance from the entrance boundary to the injector center.

The calculation was done on the staggered spatial grid $101 \times 81 \times 81$, $\Delta x = 0.14 \div 0.6$, $\Delta y = 0.07 \div 0.4$, $\Delta z = 0.03 \div 0.2$, which was chosen during the numerical experiments on the effect of number of nodes on the convergence. The table 1 below shows the sensitivity of the rate of convergence relatively to the grid characteristics by estimating the integral

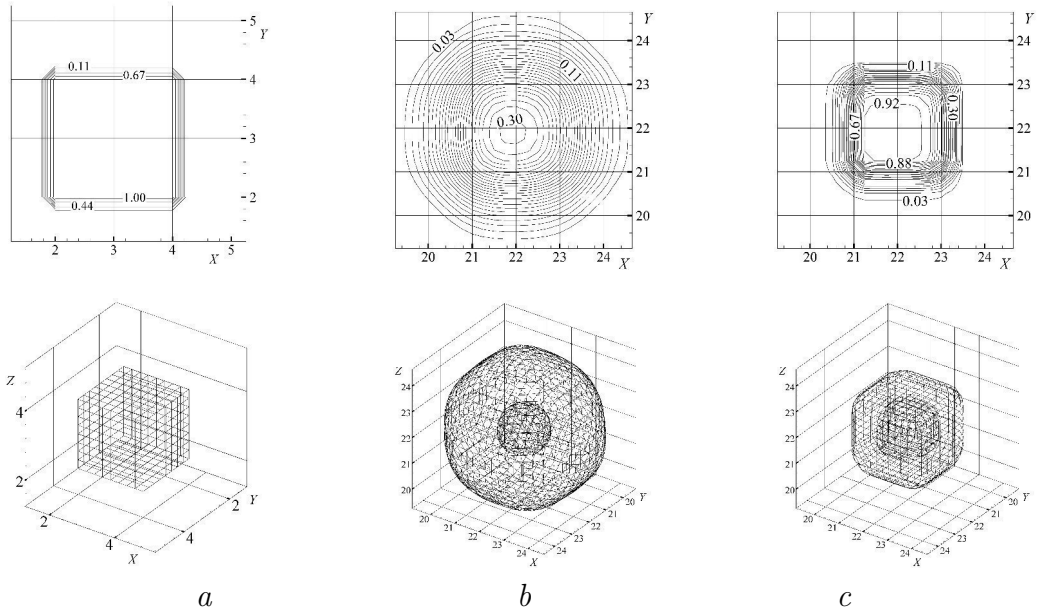

Figure 3. Numerical solution of substance balance equation: a - initial distribution, b, c - distribution at the time moment $t = 19$ ($N = 950$, $\frac{\Delta t}{\Delta x} = 0.08$) for limiters ($7a$) and ($7b$), respectively.

$L_1^\rho = \frac{1}{N}\sum_{n=1}^{N}\left|e_M^n - e_{\hat{M}}^n\right|$ and the root-mean-square $L_2^\rho = \frac{1}{N}\sqrt{\sum_{n=1}^{N}\left|e_M^n - e_{\hat{M}}^n\right|^2}$ deviations of the norm of the residuals of gas densities. Here, $M = I \times J \times K$, $\hat{M} = I \times J \times K$ – compare grids, $e_M^n = \max\limits_{(i,j,k)\in M}\left|\rho_{ijk}^{n+1} - \rho_{ijk}^n\right|$ is the norm of the residuals of gas densities, N is the number of iterations.

As follows from the table 1, the differences in the deviations of quantities reduces with the grid refinement. In accordance with this, the grid M with $101 \times 81 \times 81$ nodes was chosen since it represents a good compromise between the accuracy and the required stability condition. Fig. 4 shows the dynamics of numerical solution convergence with the use of different limiters (7) on the chosen grid, viz. the dimensionless residual norm for the gas density vs. the number of iterations N.

Table 1. Dependence of the integral and the root-mean-square deviations (the differences of the density) on nodes number

M	$\hat{M}$	L_1^ρ	L_2^ρ
$101 \times 81 \times 81$	$121 \times 101 \times 101$	$4.154 \cdot 10^{-3}$	$1.112 \cdot 10^{-4}$
$121 \times 101 \times 101$	$141 \times 121 \times 121$	$3.197 \cdot 10^{-3}$	$9.171 \cdot 10^{-5}$

Since accurate computation of mass fraction distribution is an important issue for combustion modeling, Figs. 5 and 6 give distribution of the hydrogen mass fraction in the symmetry section XZ and in the different sections XY, respectively. Here, results obtained by making use of the limiters ($7a$) are shown on the left, and the results for ($7b$) are shown on the right. It can be seen that spreading of the solution is well observable by the regions of the maximum and minimum values ($Y_1 = 0.99,\ Y_1 = 0.01$).

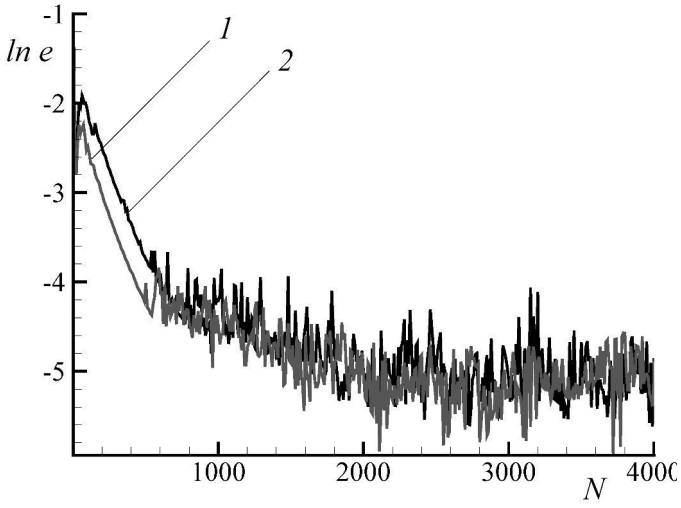

Figure 4. Dynamics of reduction of the dimensionless residual norm for the gas density, grid $101 \times 81 \times 81$, $\Delta t = 0.01$: curve *1* – for the limiters $(7a)$, curve *2* – for the limiters $(7b)$

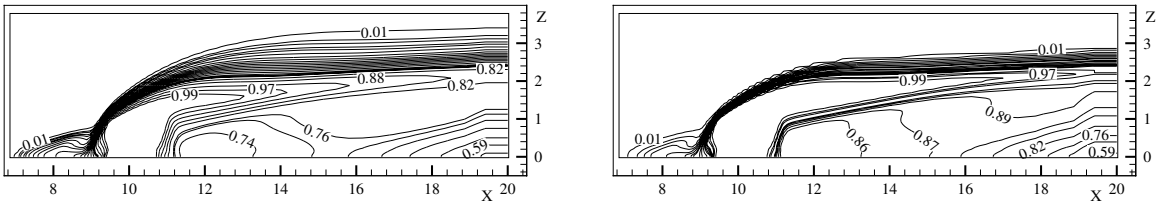

a *b*

Figure 5. Distribution of the hydrogen mass fraction in the symmetry section XZ for the limiter functions $(7a)$ (a) and $(7b)$ (b)

According to the comparison of Figs. 5 and 6 jet expansion in XZ is considerably less than that in XY. It occurs because of the great drift of the injected substance by the main flow. Also it can be noticed that making use of $(7a)$ brings about a significant increase of the solution spreading. Thus, the maximum value of height for 1% hydrogen concentration is $z_{max} = 3.41$ for $(7a)$ and $z_{max} = 2.86$ for $(7b)$.

Fig. 6a-b shows that noticeable lateral jet expansion takes place near the wall, i.e. in the subsonic region. Then the region of separation zone in front of the jet reduces due to the reduction of the subsonic boundary layer, and gets closer to the jet injection. According to this the region of the streamlined by the main flow jet contracts (Fig. 6c-d). Then the separation zone in front of the jet disappears (Fig. 6e-f), which evidences of the presence of both the lateral overflow and the jet streamlining by the airflow from above. In XY sections significant solution spreading is also can be seen for $(7a)$ in comparison with the results for $(7b)$.

Conclusion

The numerical method of the Reynolds averaged Navier-Stokes equations for the multispecies gas flow solution developed by authors in [4], based on the third order ENO scheme is adapted

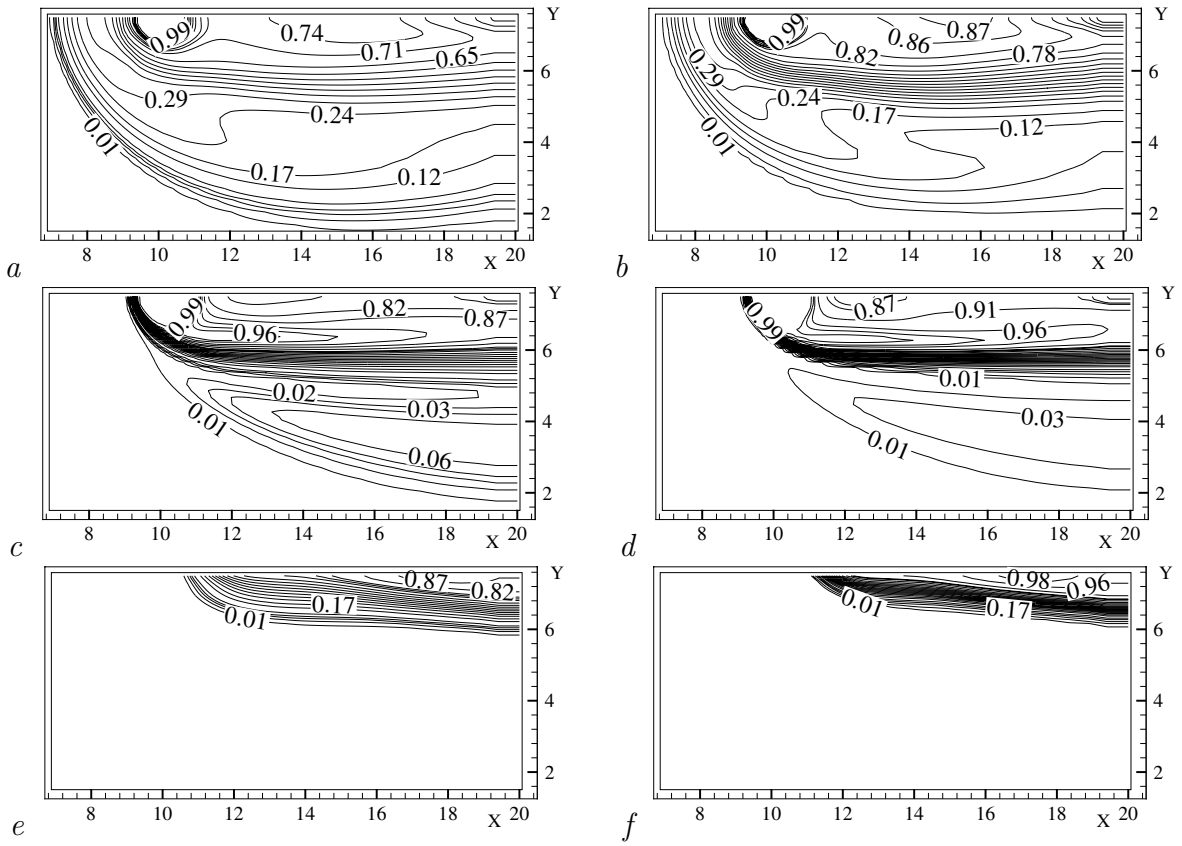

Figure 6. Distribution of the hydrogen mass fraction in the different sections XY: at $z/d = 0.3$ with (7*a*) (*a*) and (7*b*) (*b*); at $z/d = 0.82$ with (7*a*) (*c*) and (7*b*) (*d*); at $z/d = 2.18$ with (7*a*) (*e*) and (7*b*) (*f*).

for the three-dimensional case. It was obtained that the chosen limiter function, preserving the profiles for the one-dimensional case, is not appropriate for the multidimensional problems. By numerical experiments the effect of the limiters on the shock-wave structure formation and on the mixing layer was studied. As result, the optimal function which produces the smallest spread of the solution for the spatial problem was defined.

References

[1] *Adams N.A., Shariff K.* A High-Resolution Hybrid Compact-ENO Scheme for Shock-Turbulence Interaction Problems // Journal of Computational Physics, Volume 127, Issue 1, August 1996, pp. 27–51

[2] *Sun De-chuan, Hu Chun-bo, Cai Ti-min* Computation of Supersonic Turbulent Flowfield with Transverse Injection // Applied Mathematics and Mechanics. English Edition. Vol.23, No 1, Jan 2002. pp. 107-113

[3] *Amano R.S., Sun D.* Numerical Simulation of Supersonic Flowfield with Secondary Injection // The 24th Congress of ICAS, September 2004, Yokohama, pp. 1–8

[4] *Bruel P., Naimanova A. Zh.* Computation of the normal injection of a hydrogen jet into a supersonic air flow // Thermophysics and Aeromechanics, Vol. 17 issue 4 December 2010. pp. 531–542

[5] *A.KulikovskiiA.G., Pogorelov N.V., Semenov A.Yu.* Mathematical Aspects of Numerical Solution of Hyperbolic Systems. Moscow:Fizmatlit, 2001. 656 p.

[6] *Harten A.* High resolution schemes for hyperbolic conservation laws // J. Comp. Phys., Vol. 49, 1983, pp. 357-393

[7] *Harten A., Engquist B., Osher S., Chakravarthy S.* Uniformly high-order accurate essentially non-oscillatory schemes III // J. Comput. Phys., Vol. 71, 1987, pp. 231-303

[8] *Shu C., Osher S.* Efficient implementation of essentially non-oscillatory shock-capturing schemes // J. Comp. Phys. 1988. Vol. 77. pp. 439–471.

[9] *Shu C., Osher S.* Efficient implementation of essentially non-oscillatory shock-capturing schemes, II // J. Comp. Phys. 1989. Vol. 83. pp. 32–78.

[10] Berger M.J., Aftosmis M.J., Murman S.E. Analysis of slope limiters on irregular grids // In 43rd AIAA Aerospace Sciences Meeting, Reno, NV , 2005. Paper AIAA 2005-0490. pp.22

[11] *Poinsot T.J., Lele S.K.* Boundary conditions for direct simulation of compressible viscous flows // J. Comp. Phys. 1992. Vol. 101. pp. 104–129.

[12] Sweby, P.K. High resolution schemes using flux-limiters for hyperbolic conservation laws // SIAM J. Num. Anal. 1984. Vol. 21, No 5. pp. 995–1011

[13] *Danaila I., Joly P., Kaber S.M., Postel M.* Introduction to scientific computing: twelve projects solved with MATLAB // Springer, 2007. 308 p.

[14] *Harten A.* The artificial compression method for computation of shocks and contact discontinuities. III. Self-adjusting hybrid schemes // Math. Comp. 1978. Vol. 32. pp. 363–389 .